Materials Science in Semiconductor Processing 182 (2024) 108585

Contents lists available at ScienceDirect

Materials Science in Semiconductor Processing

journal homepage: www.elsevier.com/locate/mssp

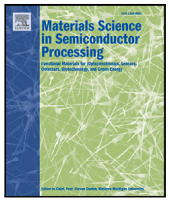

Controlled integration of InP nanoislands with CMOS-compatible Si using nanoheteroepitaxy approach

Anagha Kamath [a,*], Diana Ryzhak [b], Adriana Rodrigues [a], Navid Kafi [a], Christian Golz [a], Davide Spirito [b], Oliver Skibitzki [b], Luca Persichetti [c,d], Martin Schmidbauer [e], Fariba Hatami [a]

[a] Institut für Physik, Humboldt Universität zu Berlin, Newtonstr. 15, 12489 Berlin, Germany
[b] IHP-Leibniz Institut für Innovative Mikroelektronik, Im Technologiepark 25, 15236 Frankfurt (Oder), Germany
[c] Dipartimento di Scienze, Università degli Studi Roma Tre, Viale G. Marconi 446, Roma 00146, Italy
[d] Dipartimento di Fisica, Università di Roma "Tor Vergata", Via Della Ricerca Scientifica 1, Roma 00133, Italy
[e] Leibniz Institut für Kristallzüchtung, Max-Born-Str. 2, 12489 Berlin, Germany

ARTICLE INFO

Keywords:
Indium phosphide
Silicon nanotips
CMOS technology
Nanoheteroepitaxy
Optoelectronics

ABSTRACT

Indium phosphide (InP) nanoislands are grown on pre-patterned Silicon (001) nanotip substrate using gas-source molecular-beam epitaxy via nanoheteroepitaxy approach. The study explores the critical role of growth temperature in achieving selectivity, governed by diffusion length. Our study reveals that temperatures of about 480 °C and lower, lead to parasitic growth, while temperatures about 540 °C with an indium growth rate of about 0.7 Å.s^{-1} and phosphine flux of 4 sccm inhibit selective growth. The establishment of an optimal temperature window for selective InP growth is demonstrated for a temperature range of 490 °C to 530 °C. Comprehensive structural and optical analyses using atomic force microscopy, Raman spectroscopy, x-ray diffraction, and photoluminescence confirm a zincblende structure of indium phosphide with fully relaxed islands. These results demonstrate the capability to precisely tailor the position of InP nanoislands through a noncatalytic nanoheteroepitaxy approach, marking a crucial advancement in integrating InP nanoisland arrays on silicon devices.

1. Introduction

Silicon (Si), hailed as the backbone of modern electronic technology, has paved the path for a wide range of applications. However, it faces inherent challenges in the field of optoelectronics due to its indirect bandgap. III–V semiconductors, particularly indium phosphide (InP), has emerged as a prime candidate for integration with Si due to its efficient light emission and absorption properties, which are advantageous in devices like photodetectors, lasers, and solar cells [1–3]. Its high mobility carrier transport has proven to be crucial in high-speed transistors and communication devices [4]. The monolithic integration of InP on Si opens avenues for diverse applications, ranging from telecommunications to integrated photonics. However, achieving high-quality InP on Si poses a challenge, due to the structural and thermal expansion mismatch.

A few attempts were made towards the heterogeneous growth of InP nanostructure on Si. The vapor–liquid–solid (VLS) technique has emerged as a pivotal method for this integration [5,6]. The VLS mechanism operates on the principle of a catalytic droplet, typically gold, which acts as a nucleation center for the deposition of InP. The metal catalyst absorbs the precursors, forming a liquid alloy droplet on the silicon surface. Under optimal conditions, the alloy droplet supersaturates, leading to the nucleation and subsequent growth of InP nanowires or nanoislands. Despite these advancements, the integration of VLS-grown InP structures with standard complementary metal–oxide–semiconductor (CMOS) processes remains a notable challenge.

Nanoheteroepitaxy (NHE), a catalyst-free approach, presents a solution to the challenges associated with the growth of InP nanostructures on Si substrates. This innovative approach leverages pre-patterned Si nanotip (NT) structures, masked with silicon dioxide (SiO_2) or silicon nitride (Si_3N_4), to achieve site-specific, selective growth [7,8]. NHE introduces several crucial features, among which the compliance effect stands out. This effect plays a pivotal role in the elastic relaxation of the epitaxial layer by distributing the strain between the layer and the underlying substrate [9,10]. Additionally, NHE exhibits the capability for precise site determination, offering control and accuracy in the growth process [11]. Another noteworthy aspect is the reduction of interface defects facilitated by the smaller interface area, resulting in fewer anti-phase domain defects. These features collectively position NHE as an

* Corresponding authors.
E-mail addresses: anagha.kamath@physik.hu-berlin.de (A. Kamath), hatami@physik.hu-berlin.de (F. Hatami).

https://doi.org/10.1016/j.mssp.2024.108585
Received 25 December 2023; Received in revised form 28 May 2024; Accepted 29 May 2024

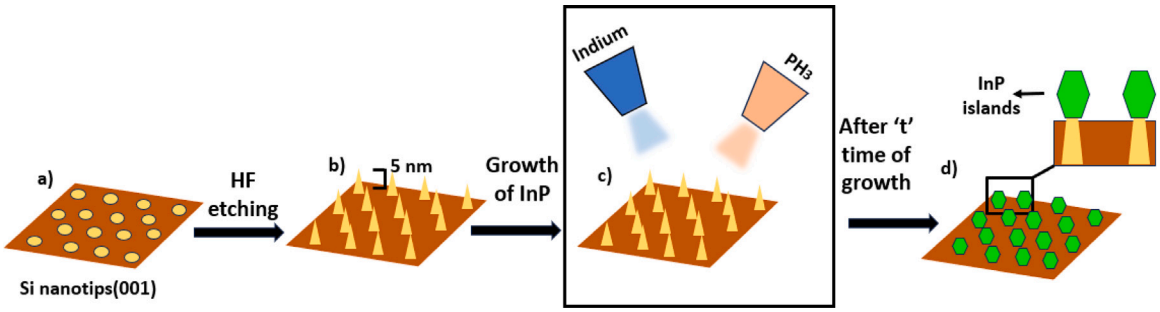

Fig. 1. Schematic of the growth process of InP on pre-patterned Si NT (001) substrate. (a) Si NTs (001) embedded in a SiO_2 layer. (b) Open Si tips after HF cleaning, serving as nucleating sites. (c) Substrate exposed to indium and phosphine for growth. (d) InP crystals growing on Si nanotips. The magnified image depicts a schematic of the cross-sectional view of the InP growth on the nanotips.

effective approach for achieving controlled and high-quality epitaxial growth. Successful realization of selective growth of nanoislands has been previously demonstrated by Niu et al. showing the growth of the InP epitaxial layer possessing bulk-like properties [12].

In this study, we use the NHE method to understand how growth temperature affects the selectivity of InP nanoislands on Si NTs. We identify the effect of temperature on size by exploring the average top-view area of the nanoislands for a range of samples. Our investigation extends to morphological, structural, and optical properties, using various spectroscopic techniques, setting the stage for potential applications in advanced optoelectronics.

2. Methodology

The methodology for growing InP on Si NT (001) substrate using the NHE approach is illustrated in Fig. 1. Fig. 1(a) provides an overview of the starting material, a 200 mm Si(001) wafer with a matrix of Si NTs. The nanotips were crafted using a multi-step procedure through the utilization of a pilot line, featuring state-of-the-art 0.13-μm bipolar CMOS technology. The NTs are arranged in a hexagonal lattice with a tip-to-tip distance of 1500 nm embedded in a SiO_2 layer. The fabrication process included SiO_2 and Si_3N_4 deposition, lithography, dry etching, and wet etching. Then, Si NTs were fully encapsulated in 1000 nm high-density plasma (HDP) oxide. The HDP oxide, recognized for its superior quality, was achieved through plasma-enhanced chemical vapor deposition with silane as the silicon precursor. The fabrication process concluded with a chemical–mechanical polishing step to thin down the SiO_2 layer, revealing a circular Si (001) NT surface with diameters ranging from 40 to 70 nm and a height of 500 nm. Additional information on the NT fabrication process can be found elsewhere [9].

Ex-situ sample preparation before growth involved removing organic residues using a Piranha-based cleaning process, followed by a 20 s dip in 0.8% hydrogen fluoride (HF) solution to remove the top layer of SiO_2. This exposed the 5 nm height of the Si NTs, serving as a seed for InP nanoisland growth. Fig. 1(b) shows the schematic of etched Si tips which are now free for the growth of InP. The substrate was then transferred to the pre-growth chamber of the gas-source molecular-beam epitaxy (GS-MBE) system, where it was heated at 200 °C to remove water-based contamination. It was then transferred to the growth chamber, where it underwent a thermal cleaning procedure, as demonstrated previously, to remove native oxides from the surface, before the deposition of InP [12]. Then, as shown schematically in Fig. 1(c), InP nanostructures were deposited on these Si NT substrates inside a gas-source MBE Riber 32-P system using solid-source indium and thermally cracked phosphine. Under optimized growth conditions, selective nucleation of InP on Si NTs was achieved. Fig. 1(d) shows a schematic of fully-grown InP nanoislands on the tips. The magnified figure depicts the schematic cross-sectional view.

The size distribution of InP nanoislands was examined through scanning electron microscopy (SEM) employing the Pioneer Two system by Raith Fabrication. To quantify the average top-view area of the nanoislands, a self-written Python script was used. Further morphological insights were obtained using Atomic Force Microscopy (AFM) with a Bruker Dimension Icon-Bruker system. AFM measurements were conducted with Bruker super sharp TESP-SS cantilevers, resonating at approximately 320 kHz, and tips featuring a radius of curvature <5 nm. Standard tapping mode was employed, and measurements were carried out under ambient conditions.

Structural analyses were pursued through high-resolution X-ray diffraction (HR-XRD) using a Bruker D8 Discover system. A pre-collimating parabolic mirror was employed in combination with an asymmetric two-bounce Ge 220 crystal monochromator ensuring a collimation of better than 0.01° at a fixed wavelength of $\lambda = 1.5406$ Å. Raman spectroscopy was performed using the Renishaw inVia system. The detector employed was the Renishaw Centrus 2K2H03-1040 × 256, and excitation was achieved with a diode-pumped solid-state laser at 532 nm, featuring a grating of 2400 lines per millimeter. The system boasted a 1 μm spot size, with an excitation beam power of 0.13 mW. The spectral resolution was maintained at 1 cm^{-1}, and the slit aperture was 65 μm. Luminescence was probed through photoluminescence (PL) employing a UV laser with a wavelength of 325 nm, a grating of 1800 grooves/mm, and a UV detector - Synapse/Symphony II Si detector. The spectra were measured in the temperature range of 80–260 K. The reflective objective at 15x magnification featured a 2 μm spot size, offering insights into the characteristics of the InP nanoislands.

3. Results and discussion

In this section, we discuss the effects of temperature on the growth of InP crystals, and the structural, morphological, and optical characteristics of InP nanoislands on Si NT substrates. Parameters such as growth temperature, and flux of group III and group V adatoms play pivotal roles in determining the boundaries of selective growth.

First, we investigate the influence of growth temperature on the position-controlled growth of InP. Several InP samples were grown on Si NTs, where growth temperature (T_G) was varied and other parameters were kept constant (PH_3 flux of 4 sccm, indium growth rate of 0.7 Å.s^{-1}, and growth time of 90 min). Fig. 2(a–e) show the top-view SEM images of samples with growth temperatures ranging from 480 °C to 540 °C. Notably, at lower temperatures (T_G = 480 °C), non-selective growth was evident, with parasitic growth observed in the SiO_2 region. From 505 °C to 525 °C, however, selective growth was noted. At temperatures around 540 °C, no growth was observed, as shown in Fig. 2(e). Fig. 2(f) shows the plot for the average top-view area of the selectively grown InP nanoislands for three selectively grown samples (Fig. 2(b–d)). We observe that the size of the islands increases from 505° to 515 °C, and then decreases as we go from 515 °C to 525 °C.

To understand the temperature-dependent behavior of InP growth on the substrate, we look at the formation process involving adsorption, nucleation, diffusion, and desorption. Our observations reveal

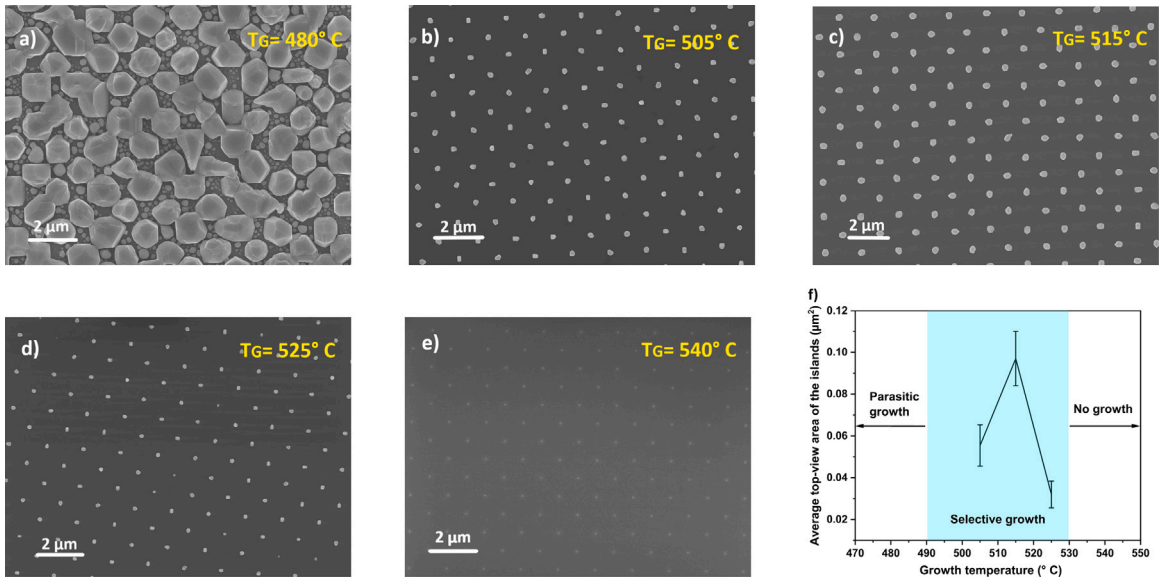

Fig. 2. Top-view SEM images of InP growth on Si NT substrates at different temperatures: (a) T_G = 480 °C, (b) T_G = 505 °C, (c) T_G = 515 °C, (d) T_G = 525 °C, and (e) T_G = 540 °C. (f) Average top-view area of the selectively grown nanoislands with corresponding growth temperatures. Standard deviation in the area is represented using error bars. The blue rectangular area depicts the window for selective growth of InP nanoislands at a PH_3 flux of 4 sccm, indium growth rate of 0.7 Å s^{-1} and 90 min of growth time.

distinct behaviors at lower growth temperatures. We identify it as parasitic growth, where InP also grows on SiO_2 region. This observed phenomenon is attributed to the diminished thermal energy available for surface diffusion processes. At lower temperatures, insufficient energy hinders atoms or molecules from overcoming activation energy barriers, thereby limiting their effective diffusion on the substrate surface [13,14]. It has been observed that this, in turn, enhances the sticking coefficient of group-III adatoms with SiO_2 [15]. Heyn demonstrated that the sticking coefficient of In adatoms on SiO_2 approaches unity at temperatures below 500 °C [16]. The parasitic growth in Fig. 2(a) suggests a low diffusion length and a high sticking coefficient of indium adatoms.

As the substrate temperature is increased, the thermal energy facilitates surface diffusion, allowing atoms to migrate more freely on the substrate. This enhanced diffusion length contributes to selective growth by enabling preferential nucleation at sites with lower surface energy. Fig. 2(f) shows the average top-view area of the selectively grown nanoislands. Beyond 515 °C, the size of the islands reduces, and ultimately at 540 °C, no growth was observed which suggests a higher desorption rate of adatoms. For the given PH_3 flux and indium growth rate, our data indicates an optimal window from 490 °C to 530 °C that shows the selective growth of InP.

Transitioning from our exploration of temperature's impact on InP nanoisland growth, we aim to understand their shapes and atomic structure. Surface energy guides the crystal towards energetically favorable orientations. As a result of the minimization, the crystal is reshaped, with facets developing as it expands. Before proceeding with the facet analysis, it is essential to establish the crystalline nature of the nanocrystals. The preliminary confirmation of the mono-crystalline nature of the nanoislands which is discussed in detail in the subsequent section of XRD analyses serves as a foundational step before exploring the intricacies of facet development.

Gaining an understanding of facet development is essential in growing nanocrystals with specific shapes, which is crucial for achieving desired material properties and characteristics. Here, we evaluate and study the morphology of one of the selectively grown InP samples using AFM [17,18]. A 2D stereographic image is shown in Fig. 3(a), which sheds light on the local normal orientations with respect to the substrate plane (001). With the substrate orientation at the center, the intensity in the picture depicts the distribution of facets. The investigation included more than 500 islands spread over several 10 × 10 μm^2 zones. Three different facet families are seen in Fig. 3(a): 72–78° (represented by white rectangles), 47–54° (highlighted by yellow circles), and 21–25° (indicated by red triangles) with respect to the (001) direction. The corresponding facet planes are mentioned in Fig. 3(a). The local gradient image of a single InP nanoisland is shown in Fig. 3(b), which displays the complex facet landscape. The shallowest 22° facet is positioned at the island's top, while steeper facets at 55° and ultra-steep facets at 75° are evident towards the island's base. Notably, islands exhibiting (313) and (111) facets demonstrate the highest packing density, while (205) facets exhibit the lowest, as depicted in Fig. 3(c).

The size and distribution of the islands are further studied by statistical analysis of AFM images. Fig. 3(d) and (e) depict the distribution profiles of two key parameters, namely the zero-basis volume and the equivalent disc radius respectively, obtained from measurements of approximately 200 islands. The zero-basis volume represents the volume encapsulated by the island defined by its grain boundary. As illustrated in Fig. 3(d), the distribution of zero basis volumes reveals the variability in island sizes across the sample. Concurrently, the equivalent disc radius is a measure of a hypothetical circular disc that would have the same area as the selectively grown island. We use this concept to simplify the representation of irregularly shaped islands, allowing for more straightforward analysis and comparison. The distribution of the disc radius of islands is presented in Fig. 3(e). The mean zero basis volume of the islands is calculated to be 34 × 10^6 nm^3. Simultaneously, the mean equivalent disc radius is determined to be 277 nm, representing the average two-dimensional size of the islands. Understanding these physical dimensions of the nanostructures is crucial for predicting their optical and electronic behaviors.

Moving beyond the topographical features revealed by AFM, we now shift our investigation towards unraveling the crystallographic structures within these InP nanoislands. This involves an investigation of the crystal phase structure through the complementary techniques of XRD and Raman spectroscopy. Figure 4(a) presents a $2\theta/\theta$ scan covering a broad angular range, acquired from a large ensemble of nanoislands. Alongside the Si (004) and the basis-forbidden Si (002) reflection peaks [19], two additional well-resolved Bragg diffraction peaks emerge at 2θ = 30.45° and 63.37°. These correspond to the cubic zincblende (ZB) InP (002) and (004) Bragg reflections, respectively [20,21]. Notably, the lattice parameter of a = 5.866 Å, as evaluated from the InP (002) and (004) peak positions, suggests a fully relaxed InP

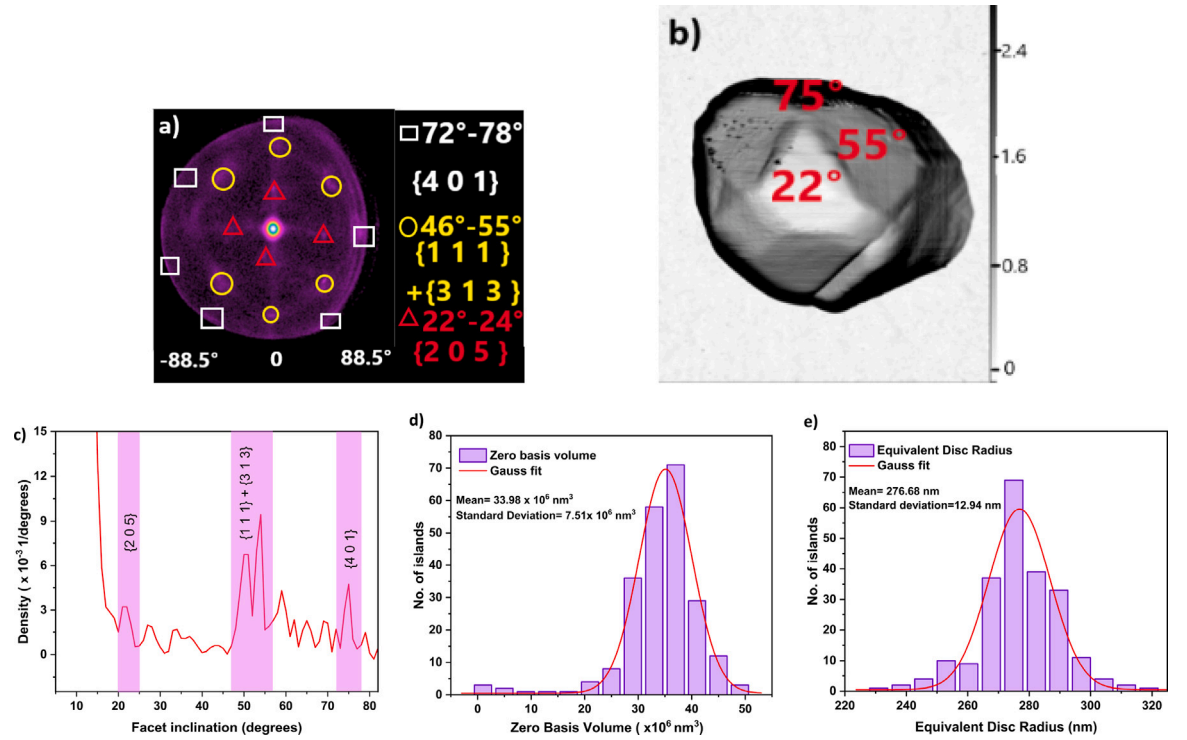

Fig. 3. (a) 2D stereographic image showing the facets calculated for over 500 InP nanoislands. The orientation between 72–78° is represented by white rectangles, 47–54° highlighted by yellow circles, and 21–25° by red triangles with respect to the (001) direction. The corresponding facet planes are mentioned. (b) Local gradient image showing the preferential facets of a single nanoisland. The shallowest 22° facet is positioned at the island's top, while steeper facets at 55° and ultra-steep facets at 75° are evident towards the island's base. (c) The facets analyzed from around 500 nanoislands with the highest density are highlighted in purple. (d) the distribution of volume basis of around 200 InP nanoislands, fitted with Gaussian function. (e) The distribution of disc radius calculated for over 200 nanoislands.

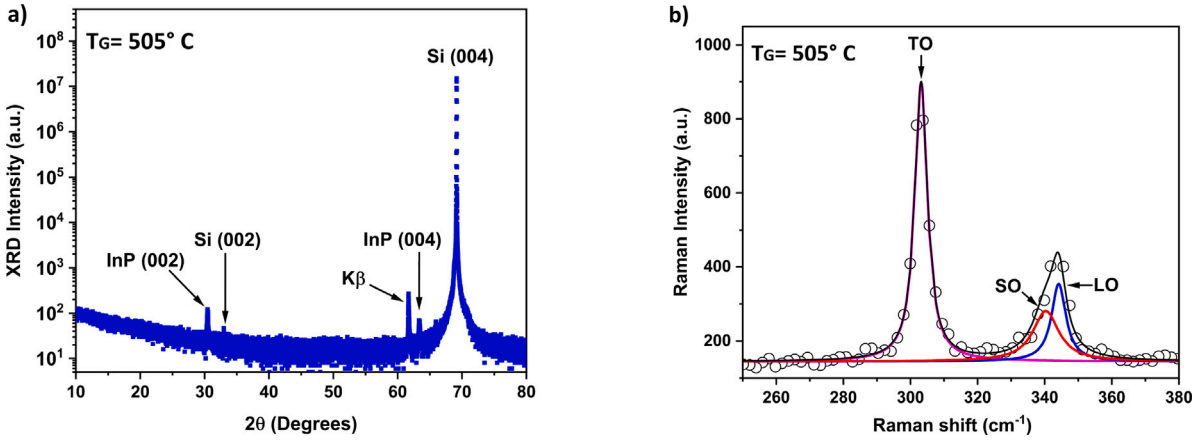

Fig. 4. (a) 2θ XRD showing InP(002) and (004) peak at $2\theta = 30.5°$ and 63.2° respectively. (b) Raman spectra at room temperature, fitted by Lorentzian function, show TO, LO and SO modes of InP at 303.07 cm^{-1}, 344.5 cm^{-1}, and 340.06 cm^{-1} respectively, indicating strain-free ZB InP crystal structure.

crystal with no discernible epitaxial strain. Please note that the low-intensity peak at $2\theta = 61.69°$ (labeled 'Kβ') corresponds to the Si (004) substrate Bragg reflection excited by a weak fraction of Cu Kβ radiation ($\lambda = 1.392$ Å). Furthermore, there is no indication of the hexagonal InP wurtzite phase in the diffractogram.

To further validate the observation of strain-free ZB InP, Raman measurements were conducted as illustrated in Fig. 4(b). Employing the Lorentzian function for peak fitting, we find a peak at 303.07 cm^{-1}, and a spectral feature composed of two peaks at 340.06 cm^{-1} and 344.5 cm^{-1}. The peaks at 303.07 cm^{-1} and 344.5 cm^{-1} correspond very well with the expected transverse optical (TO) and longitudinal optical (LO) phonon modes of ZB InP [22]. Simultaneously, the observed peak at 340.06 cm^{-1} suggests a potential contribution from surface optical (SO) modes [23]. This combined Raman and XRD spectroscopy investigation clarifies the InP islands possess cubic ZB structures and are fully relaxed.

The insights gained from the structural characterization of selectively grown undoped InP nanoislands lay the foundation for considering potential applications in optoelectronic devices. We further shift our focus to optical characteristics, particularly luminescence behavior, for light-emitting applications. Fig. 5(a) presents the temperature-dependent PL spectra in a semi-logarithmic axis, covering a range from 80 K to 260 K. It is important to note that no photoluminescence was observed at room temperature. At 80 K, two distinct peaks, labeled X and Y, are observed. Peak X appears as a broad shoulder at 1.38 eV, while Peak Y stands out with a sharp and distinct emission at 1.41 eV. Notably, Peak X becomes indistinguishable as temperatures rise above 80 K, and Peak Y experiences a redshift.

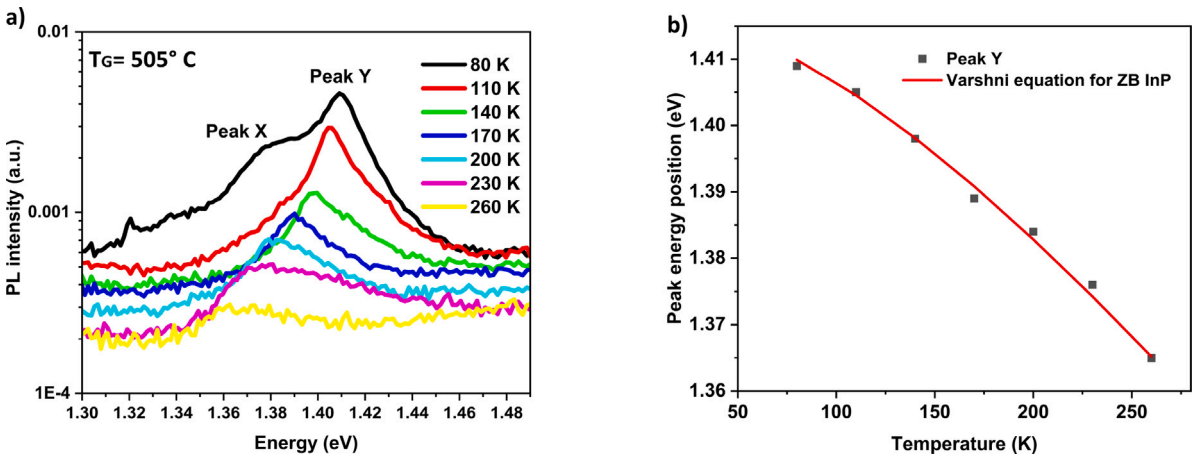

Fig. 5. (a) Temperature-dependent PL spectra from 80 K to 260 K with a laser excitation source of 325 nm depicting peak X and peak Y at 1.38 eV and 1.41 eV respectively. (b) Energy positions of peak Y for different temperatures are fitted with the Varshni equation for ZB InP.

To ensure the accuracy of our spectral analysis, we adopted the second-derivative approach to enhance peak visibility. A smooth baseline was mathematically constructed and then subtracted from the original data, to isolate the luminescent signal. We then applied standard spectral analysis techniques to identify and differentiate the peaks accurately. In addition, the application of a smoothing technique reduced the inherent noise in the data, resulting in improved clarity of our spectral representation.

In Fig. 5(b), the plot of the peak energy position of peak Y against temperature (80 K to 260 K) reveals a redshift of 42 meV. The data fits well with the Varshni equation for ZB InP, suggesting that Peak Y is associated with the band-to-band transition of ZB InP [24].

The positioning of peak X at 1.38 eV at 80 K closely aligns with the acceptor-related transitions in InP due to Si [25,26]. Extensive evidence supporting Si's role as an acceptor in InP is found in studies by Ka et al. and Zheng et al. highlighting its incorporation into InP as an acceptor on a group V sublattice [25,27]. It is crucial to consider the potential for unintentional Si doping in InP islands. This may happen either through the interdiffusion of Si atoms from the tip to the islands or via the involvement of free Si atoms generated during the thermal cleaning process [8,28]. Hence, we attribute the presence of Peak X to acceptor-related transitions.

4. Conclusion

We have successfully demonstrated the controlled growth of InP nanoislands on pre-patterned CMOS-compatible Si NT (001) substrates using the GS-MBE technique within the nanoheteroepitaxy framework. InP growth is achieved for a constant flux of 4 sccm phosphine and an indium growth rate of about 0.7 Å.s^{-1}. We unraveled the role of temperature in achieving this selectivity, revealing that temperatures around 480 °C and below lead to parasitic growth due to limited adatom diffusion and a higher sticking coefficient of indium adatoms and SiO_2. Conversely, temperatures around 540 °C and higher hinder growth because of increased desorption rates and surface diffusion.

Further characterization through AFM indicated the preferential facets of the grown nanoislands. We observed three inclination angles; the shallowest 22° facet crowns the island, while steeper facets at 55° and ultra-steep facets at 75° mark the island's base. We have shown by XRD and Raman measurements that InP nanoislands contain elastically relaxed zincblende structures. This structural investigation provides a foundation for utilizing their optical features. PL measurements yielded strong evidence of emissions at about 1.41 eV corresponding to the signatures of zincblende InP. These findings not only enrich our understanding of the growth dynamics of InP nanoislands on CMOS-compatible Si wafer but also hold significant implications for practical applications in optoelectronics.

CRediT authorship contribution statement

Anagha Kamath: Original draft, methodology, investigation, and data analysis. **Diana Ryzhak:** PL and Raman analysis, reviewing. **Adriana Rodrigues:** SEM analysis, reviewing. **Navid Kafi:** Python Software development for statistical analysis, reviewing. **Christian Golz:** SEM analysis, reviewing. **Davide Spirito:** PL and Raman analysis, reviewing. **Oliver Skibitzki:** Supervision of PL and Raman measurements, reviewing. **Luca Persichetti:** AFM measurement and analysis, reviewing. **Martin Schmidbauer:** XRD measurements and analysis, reviewing. **Fariba Hatami:** Supervision of the research, writing.

Declaration of competing interest

The authors declare that they have no known competing financial interests or personal relationships that could have appeared to influence the work reported in this paper.

Data availability

Data will be made available on request.

Acknowledgments

A.K. thanks Deutscher Akademischer Austauschdienst (DAAD) for her research grant. This work was supported by the German Research Foundation (DFG Grant No. 428250328).

References

[1] Xin Yan, Bang Li, Qimin Lin, Peng Liu, Yanbin Luo, Qichao Lu, Xia Zhang, Xiaomin Ren, High performance transistors and photodetectors based on self-catalyzed zinc-blende InP nanowires, Appl. Phys. Lett. 114 (24) (2019).
[2] Svenja Mauthe, Yannick Baumgartner, Marilyne Sousa, Qian Ding, Marta D Rossell, Andreas Schenk, Lukas Czornomaz, Kirsten E Moselund, High-speed III–V nanowire photodetector monolithically integrated on Si, Nat. Commun. 11 (1) (2020) 4565.
[3] Nicklas Anttu, Alireza Abrand, Damir Asoli, Magnus Heurlin, Ingvar Åberg, Lars Samuelson, Magnus Borgström, Absorption of light in InP nanowire arrays, Nano Res. 7 (2014) 816–823.
[4] Katsuhiro Tomioka, Takashi Fukui, Recent progress in integration of III–V nanowire transistors on Si substrate by selective-area growth, J. Phys. D: Appl. Phys. 47 (39) (2014) 394001.
[5] Thuy TT Vu, Tilman Zehender, Marcel A Verheijen, Sébastien R Plissard, George WG Immink, Jos EM Haverkort, Erik PAM Bakkers, High optical quality single crystal phase wurtzite and zincblende InP nanowires, Nanotechnology 24 (11) (2013) 115705.
[6] Takashi Fukui, Masatoshi Yoshimura, Eiji Nakai, Katsuhiro Tomioka, Position-controlled III–V compound semiconductor nanowire solar cells by selective-area metal–organic vapor phase epitaxy, Ambio 41 (2012) 119–124.

[7] Gang Niu, Giovanni Capellini, Markus Andreas Schubert, Tore Niermann, Peter Zaumseil, Jens Katzer, Hans-Michael Krause, Oliver Skibitzki, Michael Lehmann, Ya-Hong Xie, et al., Dislocation-free Ge nano-crystals via pattern independent selective Ge heteroepitaxy on Si nano-tip wafers, Sci. Rep. 6 (1) (2016) 22709.

[8] Oliver Skibitzki, Ivan Prieto, Roksolana Kozak, Giovanni Capellini, Peter Zaumseil, Yadira Arroyo Rojas Dasilva, Marta D Rossell, Rolf Erni, Hans von Känel, Thomas Schroeder, Structural and optical characterization of GaAs nano-crystals selectively grown on Si nano-tips by MOVPE, Nanotechnology 28 (13) (2017) 135301.

[9] Gang Niu, Giovanni Capellini, Grzegorz Lupina, Tore Niermann, Marco Salvalaglio, Anna Marzegalli, Markus Andreas Schubert, Peter Zaumseil, Hans-Michael Krause, Oliver Skibitzki, Michael Lehmann, Francesco Montalenti, Ya-Hong Xie, Thomas Schroeder, Photodetection in hybrid single-layer graphene/fully coherent germanium island nanostructures selectively grown on silicon nanotip patterns, ACS Appl. Mater. Interfaces 8 (3) (2016) 2017–2026, http://dx.doi.org/10.1021/acsami.5b10336, arXiv:https://doi.org/10.1021/acsami.5b10336. PMID: 26709534.

[10] D. Zubia, S.D. Hersee, Nanoheteroepitaxy: The application of nanostructuring and substrate compliance to the heteroepitaxy of mismatched semiconductor materials, J. Appl. Phys. 85 (9) (1999) 6492–6496.

[11] Anagha Kamath, Oliver Skibitzki, Davide Spirito, Shabnam Dadgostar, Irene Mediavilla Martinez, Martin Schmidbauer, Carsten Richter, Albert Kwasniewski, Jorge Serrano, Juan Jimenez, et al., Monolithic integration of InP nanowires with CMOS fabricated silicon nanotips wafer, Phys. Rev. Mater. 7 (10) (2023) 103801.

[12] Gang Niu, Giovanni Capellini, Fariba Hatami, Antonio Di Bartolomeo, Tore Niermann, Emad Hameed Hussein, Markus Andreas Schubert, Hans-Michael Krause, Peter Zaumseil, Oliver Skibitzki, et al., Selective epitaxy of InP on Si and rectification in graphene/InP/Si hybrid structure, ACS Appl. Mater. Interfaces 8 (40) (2016) 26948–26955, http://dx.doi.org/10.1021/acsami.6b09592.

[13] Vladimir G. Dubrovskii, Criterion for selective area growth of III–V nanowires, Nanomaterials 12 (20) (2022) 3698.

[14] Martin Setvín, Jakub Javorskỳ, Zsolt Majzik, Pavel Sobotík, Pavel Kocán, Ivan Ošťádal, Competition between thermally activated and tip-induced hopping of indium atoms on Si (100), Phys. Rev. B 85 (8) (2012) 081403.

[15] Martin Heiß, Eva Riedlberger, Danče Spirkoska, Max Bichler, Gerhard Abstreiter, Anna Fontcuberta i Morral, Growth mechanisms and optical properties of GaAs-based semiconductor microstructures by selective area epitaxy, J. Cryst. Growth 310 (6) (2008) 1049–1056.

[16] Ch Heyn, Stability of InAs quantum dots, Phys. Rev. B 66 (7) (2002) 075307.

[17] Petr Klapetek, David Necas, Christopher Anderson, Gwyddion user guide, Czech Metrol. Inst. 2007 (2004) 2009.

[18] David Nečas, Petr Klapetek, Gwyddion: an open-source software for SPM data analysis, Open Phys. 10 (1) (2012) 181–188.

[19] Peter Zaumseil, High-resolution characterization of the forbidden Si 200 and Si 222 reflections, J. Appl. Crystallogr. 48 (2) (2015) 528–532.

[20] H Oomae, S Irizawa, Y Jinbo, H Toyota, T Kambayashi, N Uchitomi, Studies of zinc-blende type MnAs thin films grown on InP (001) substrates by XRD, J. Cryst. Growth 378 (2013) 410–414.

[21] MSYPM Levinshtein, Handbook Series on Semiconductor Parameters, vol. 1, World Scientific, 1997.

[22] A. Mooradian, G.B. Wright, First order Raman effect in III–V compounds, Solid State Commun. 4 (9) (1966) 431–434.

[23] N. Esser, Analysis of semiconductor surface phonons by Raman spectroscopy, Appl. Phys. A 69 (1999) 507–518.

[24] Y.P. Varshni, Temperature dependence of the elastic constants, Phys. Rev. B 2 (10) (1970) 3952.

[25] H.Q. Zheng, K. Radahakrishnan, S.F. Yoon, G.I. Ng, Electrical and optical properties of Si-doped InP grown by solid source molecular beam epitaxy using a valved phosphorus cracker cell, J. Appl. Phys. 87 (11) (2000) 7988–7993.

[26] S.F. Yoon, K.W. Mah, H.Q. Zheng, Transport and photoluminescence of silicon-doped GaInP grown by a valved phosphorus cracker cell in solid source molecular beam epitaxy, J. Appl. Phys. 85 (10) (1999) 7374–7379.

[27] O. Ka, A. Yamada, H. Yoshinaga, Y. Makita, Si acceptor excited states in ion-implanted InP, J. Appl. Phys. 78 (8) (1995) 5171–5173.

[28] DG Deppe, WE Plano, JE Baker, N Holonyak Jr., MJ Ludowise, CP Kuo, RM Fletcher, TD Osentowski, MG Craford, Comparison of SiIII-SiV and SiIII-VIII diffusion models in III–V heterostructures lattice matched to GaAs, Appl. Phys. Lett. 53 (22) (1988) 2211–2213.